



Functionalizing aromatic compounds with optical cycling centres

Guo-Zhu Zhu ¹, Debayan Mitra ^{2,3,7}, Benjamin L. Augenbraun^{2,3}, Claire E. Dickerson ⁴, Michael J. Frim³, Guanming Lao ¹, Zack D. Lasner^{2,3}, Anastassia N. Alexandrova ^{4,5}, Wesley C. Campbell^{1,5,6}, Justin R. Caram^{4,5}, John M. Doyle^{2,3} and Eric R. Hudson ^{1,5,6}

Molecular design principles provide guidelines for augmenting a molecule with a smaller group of atoms to realize a desired property or function. We demonstrate that these concepts can be used to create an optical cycling centre, the Ca(I)-O unit, that can be attached to a number of aromatic ligands, enabling the scattering of many photons from the resulting molecules without changing the molecular vibrational state. Such capability plays a central role in quantum state preparation and measurement, as well as laser cooling and trapping, and is therefore a prerequisite for many quantum science and technology applications. We provide further molecular design principles that indicate the ability to optimize and expand this work to an even broader class of molecules. This represents a great step towards a quantum functional group, which may serve as a generic qubit moiety that can be attached to a wide range of molecular structures and surfaces.

olecules and surfaces can be augmented with molecular fragments that imbue a desired property to the system. Such functionalization can determine the system reactivity and properties, allowing a host of capabilities, such as catalysis^{1,2} and biological and chemical binding and sensing^{3–5}. As the properties of the functional groups are often not strongly affected by the bonding to the host molecule, the technique can bring the same function to a wide variety of systems.

It is interesting to consider extending the idea of a functional group to new operations. For example, can a robust qubit moiety be designed to act as a functional group attached to a larger molecule? Can multiple such quantum functional groups connect through space, allowing the host compound to serve as a bus for entanglement? And, relatedly, can a quantum functional group be used to control or witness the dynamics of a larger molecular whole?

In this Article we shed light on these questions by demonstrating the key features of a quantum functional group known as an optical cycling centre (OCC). We experimentally show that a functional group, an alkaline-earth(I)-oxygen moiety, can be attached to a variety of aromatic compounds while retaining the property that it can scatter many photons without changing vibrational state. This property opens the door to using lasers to cool⁶ external and internal degrees of freedom of large molecules by simply functionalizing them with an OCC. With this capability come the prerequisites for quantum information science with large molecules, namely mechanical control and qubit-state preparation and readout.

The process for OCC functionalization can be understood intuitively by considering the neutral molecules that have previously been laser-cooled. Much success has been achieved with diatomic molecules composed of an alkaline-earth metal atom bonded to a halogen atom^{7,8}. In such molecules, the halogen atom withdraws an electron from the alkaline-earth atom, leaving one metal-centred

radical electron whose highest-occupied and lowest-unoccupied molecular orbitals (HOMO and LUMO), respectively, do not strongly participate in the molecular bonding and closely resemble those of an alkali atom. The result is a molecule that can absorb and emit many photons without changing vibrational state⁹.

More recently, this theme was demonstrated experimentally with an alkaline-earth metal atom bonded to -OH (ref. ¹⁰). It was proposed that the same approach could be used for an entire class of alkaline metal-oxide-radical molecules, including complex polyatomic molecules¹¹, and laser cooling was later extended to the -OCH₃ ligand¹². Like a halogen atom, all of these fragments withdraw an electron from the metal atom. This suggests that the alkaline-earth(I)-oxygen moiety can be considered as a functional group, akin to an alcohol or ether. Subsequent bonding of this functional group to electron-withdrawing ligands should therefore allow scattering of many photons without changing the vibrational state of the resulting molecule¹³⁻¹⁶.

To explore the limits of this concept, we studied the functionalization of aromatic compounds with an OCC. Specifically, we attached a Ca(I)—O unit to a phenyl group (-Ph) and its derivatives (-Ph-X, X=3-CH₃, 3-F, 3-CF₃, 3,4-F₂ and 3,4,5-F₃; Fig. 1a), and measured the vibronic spectra of the resulting molecules with dispersed laser-induced fluorescence (DLIF) spectroscopy. We found that the OCC transition frequency is linearly related to the acid dissociation constant (p K_a) of the precursor compound, providing a simple means for predicting molecular properties. Furthermore, the vibrational branching ratios (VBRs) were determined and, regardless of the choice of ligand, it was found that \gtrsim 90% of the photon scattering events did not change the vibrational state of the molecule. Small variation in the VBR, at the few percent level, was observed, and found to be consistent with a theoretical calculation, suggesting that p K_a provides a simple guide for designing ligands

¹Department of Physics and Astronomy, University of California, Los Angeles, CA, USA. ²Harvard-MIT Center for Ultracold Atoms, Cambridge, MA, USA. ³Department of Physics, Harvard University, Cambridge, MA, USA. ⁴Department of Chemistry and Biochemistry, University of California, Los Angeles, CA, USA. ⁵Center for Quantum Science and Engineering, University of California, Los Angeles, CA, USA. ⁶Challenge Institute for Quantum Computation, University of California, Los Angeles, CA, USA. ⁷Present address: Department of Physics, Columbia University, New York, NY, USA. [™]e-mail: hudson@physics.ucla.edu

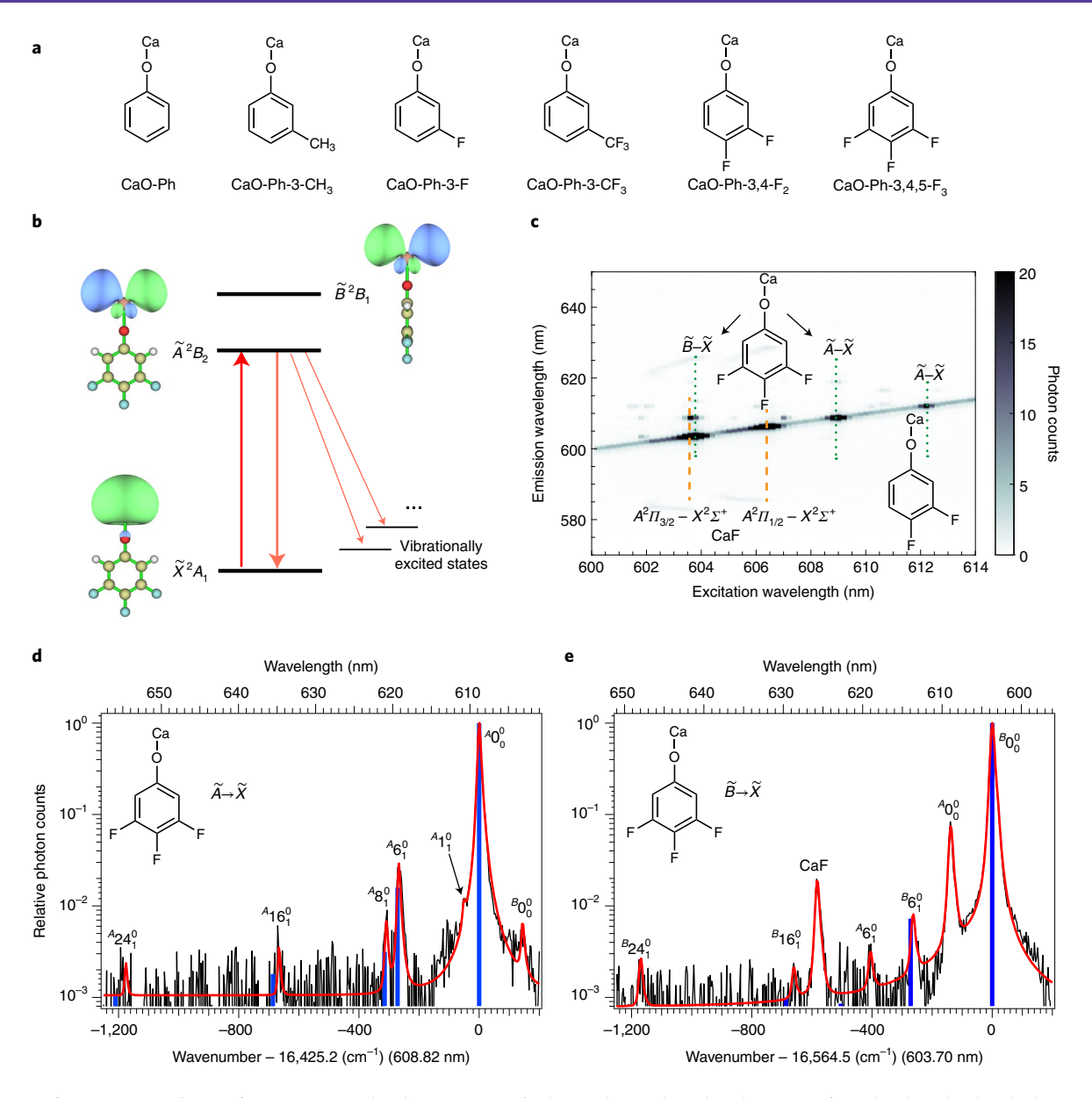


Fig. 1 | 2D and DLIF spectra of CaO-Ph-3,4,5-F₃. a, Molecular structures of calcium phenoxide and its derivatives. **b**, Molecular orbital and schematic energy levels of CaO-Ph-3,4,5-F₃. All other molecules have similar orbitals and energy levels. **c**, 2D excitation-DLIF spectrum following the reaction of Ca with 3,4,5-trifluorophenol. The orange dashed lines indicate the transition bands of CaF, and green dotted lines indicate the transition bands of CaO-Ph-3,4,5-F₃ and CaO-Ph-3,4-F₂. **d**, DLIF spectrum for the $\widetilde{A} \to \widetilde{X}$ decay of CaO-Ph-3,4,5-F₃ when excited at 608.82 nm. **e**, DLIF spectrum for the $\widetilde{B} \to \widetilde{X}$ decay of CaO-Ph-3,4,5-F₃ when excited at 603.70 nm. In **d** and **e**, the experimental spectra (black) are overlaid with Pearson distribution fits (red, see Supplementary Information for further details). The blue vertical lines indicate the calculated frequencies of the vibrational modes and the heights of the lines reflect their calculated relative strengths.

with the best OCC performance¹⁵. From this work, we found that CaO-Ph-3,4,5-F₃ does not change its vibrational state during ~99% of scattering events, implying that laser cooling is possible with current technology. In what follows, we describe the apparatus and experiments, present the recorded spectra and measured VBRs, and discuss the next steps for decorating molecules and surfaces with quantum functional groups.

The molecules were produced by the reaction of Ca atoms with ligand precursors, then cooled in a cryogenic He buffer-gas cell operated at ~9 K (ref. ¹⁷; see Methods for details). A tunable, pulsed optical parametric oscillator (OPO) provided the excitation light, and a monochromator augmented with an intensified charge-coupled device (ICCD) camera recorded the dispersed fluorescence (see Methods for further details).

Results and discussion

Two-dimensional and DLIF spectra of CaO-Ph-3,4,5-F₃. Molecular species were first identified using 2D spectroscopy, performed by scanning the OPO frequency and recording the DLIF. Transitions between the ground $(\widetilde{\chi}^2 A_1)$ and two lowest-energy electronic states $(\widetilde{A}^2 B_2 \text{ and } \widetilde{B}^2 B_1)$ have been predicted to have potential for laser cooling¹⁵ due to localization of the molecular orbitals on the Ca atom (Fig. 1b), and are therefore the targets of this work. Example data are shown in Fig. 1c for CaO-Ph-3,4,5-F₃ (the 2D spectra of all other molecules observed are shown in Extended Data Fig. 1). Four strong spectral features were observed. The excitation to the \widetilde{B} electronic state of CaO-Ph-3,4,5-F₃ is indicated by the green dotted line near 603.5 nm, and the excitation to the \widetilde{A} electronic state is at 608.5 nm. The two broad bands near 603.5 nm

NATURE CHEMISTRY ARTICLES

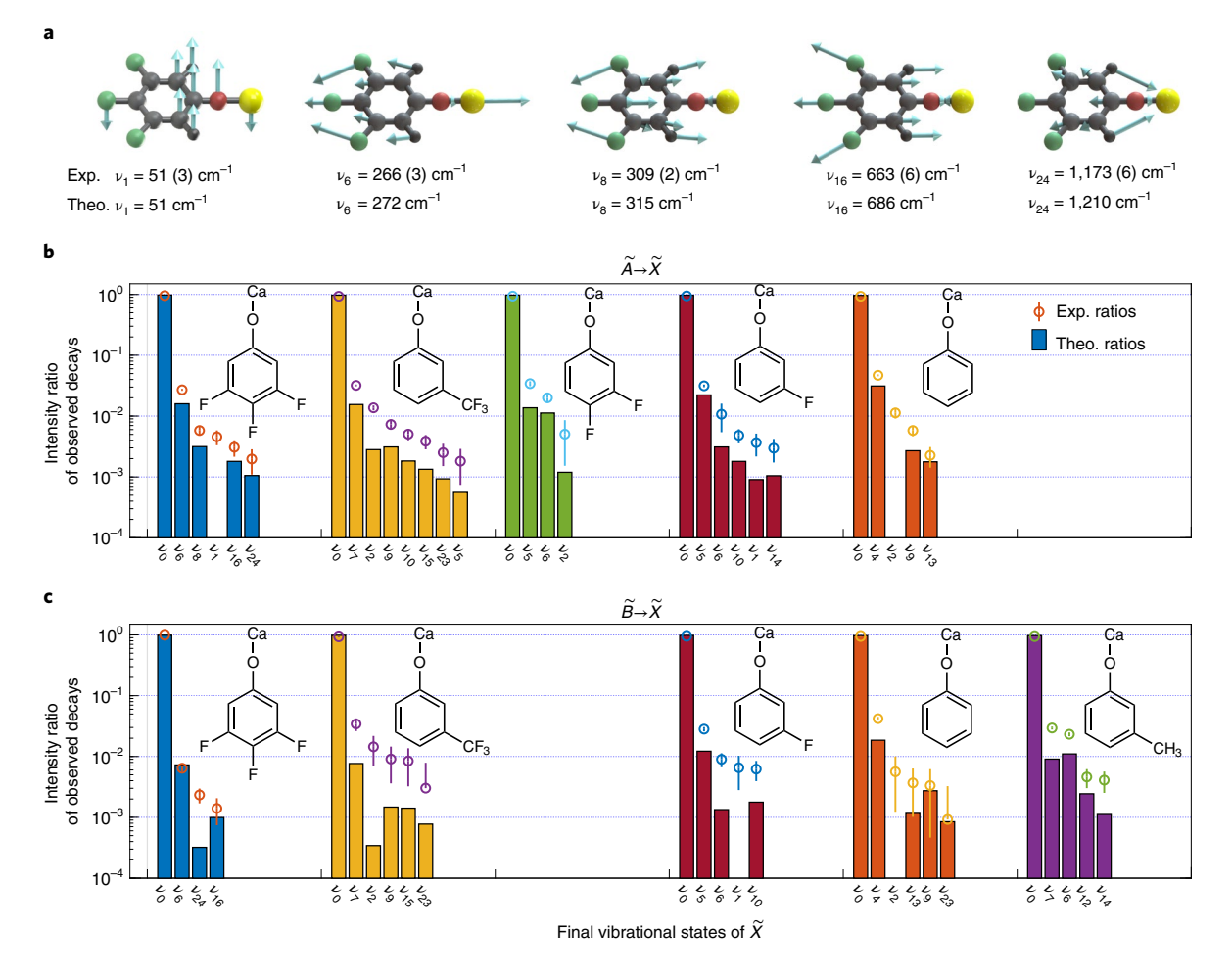


Fig. 2 | Vibrational decay ratios for all observed modes. a, The observed vibrational modes of CaO-Ph-3,4,5- F_3 , with experimentally determined and theoretical frequencies listed. The arrows indicate the direction of vibrational displacements. **b,c**, Intensity ratio of observed decays, relative to total observed decays, for $\widetilde{A} \to \widetilde{X}$ (**b**) and $\widetilde{B} \to \widetilde{X}$ (**c**) transitions, for all molecules and modes studied in this work, arranged in order of increasing pK_3 . Experimental values are denoted with circles, and calculated values are depicted as bars for clarity. Error bars (s.d.) are statistical standard errors. The vibrational mode denoted as ν_i indicates the decay to the final vibrational state of I_1^0 . The $\widetilde{A} \to \widetilde{X}$ decay of CaO-Ph-3-CH $_3$ and the $\widetilde{B} \to \widetilde{X}$ decay of CaO-Ph-3,4- F_2 are omitted due to coincidences with the CaOH and CaF decays, respectively. The values are summarized in Supplementary Table 3.

and 606.5 nm, marked by dashed orange lines, are attributed to the v'=0-v''=0 bands of the $A^2\Pi_{3/2}\leftarrow X^2\Sigma^+$ and $A^2\Pi_{1/2}\leftarrow X^2\Sigma^+$ transitions, respectively, of CaF, which is also formed when Ca reacts with a fluorinated phenol. A weaker feature at 612.0 nm is due to the $\widetilde{A}-\widetilde{X}$ transition of CaO-Ph-3,4-F₂, which is a by-product of the reaction between Ca and 3,4,5-trifluorophenol. Assignments were made by comparing the observed and calculated vibrational frequencies (Supplementary Table 1), as discussed further in the following.

Having identified the molecules, DLIF measurements were recorded by tuning the OPO to a selected resonance and accumulating between 4,000 and 8,000 ICCD exposures. Representative DLIF spectra for CaO-Ph-3,4,5-F₃ are shown in Fig. 1d,e (those of the other molecules are presented in Extended Data Fig. 1). All spectra are plotted in terms of the energy difference (in cm⁻¹) relative to the excitation energy and are normalized to the peak at the origin. The measured peak widths (full-width at half-maximum) are ~0.5 nm, mainly due to the spectrometer resolution (~0.5 nm) and the rotational distribution on decay (~0.1 nm). Figure 1d shows the DLIF spectrum of CaO-Ph-3,4,5-F₃ when exciting the $\widetilde{A} \leftarrow \widetilde{X}$ transition at 608.82 nm. The peak, labelled as $^A0_0^0$, represents the decay from the excited $\widetilde{A}(\nu'=0)$ state to the ground $\widetilde{X}(\nu''=0)$ state. The strongest vibration-changing decay, observed at $-267\,\mathrm{cm}^{-1}$ and

labelled $^{A}6^{0}_{1}$, is assigned to the Ca–O and ring-stretching mode of the \widetilde{X} state with a predicted harmonic frequency of $272\,\mathrm{cm^{-1}}$ (Fig. 2a and Supplementary Table 1). Similarly, peaks at $-309\,\mathrm{cm^{-1}}$ and $-666\,\mathrm{cm^{-1}}$ can be assigned to 8^{0}_{1} and 16^{0}_{1} , respectively, which are both symmetric stretching modes involving the benzene ring (Fig. 2a). A weak decay at $-1,175\,\mathrm{cm^{-1}}$ is attributed to the high-frequency stretching mode 24^{0}_{1} (Fig. 2a). The small shoulder next to the diagonal peak is due to decays to the lowest-frequency fundamental bending mode, 1^{0}_{1} . The vertical blue lines are the calculated VBRs normalized by the predicted value for the 0-0 decay. Interestingly, as noted by the absence of a predicted VBR for the 1^{0}_{1} peak, theoretical calculations predict this decay pathway to be negligible. The observed strength of this decay is probably due to vibronic couplings among and anharmonicities within the low-frequency modes 15,18,19 not considered in the present calculation.

The DLIF spectrum of CaO-Ph-3,4,5-F₃ from the \widetilde{B} state is shown in Fig. 1e. In addition to the non-vibration-changing decay ${}^B0^0_0$ and the dominant vibration-changing decay ${}^B6^0_1$, decays are observed with shifts of $-139\,\mathrm{cm}^{-1}$ and $-407\,\mathrm{cm}^{-1}$. These peaks are due to emissions from $\widetilde{A}(\nu'=0)$, which is presumably populated by collisional relaxation in the buffer gas^{20,21}. Interestingly, we also see evidence of collision-induced excitation when exciting to the \widetilde{A} state; as seen in Fig. 1d, a small peak at a positive shift of 140 cm⁻¹

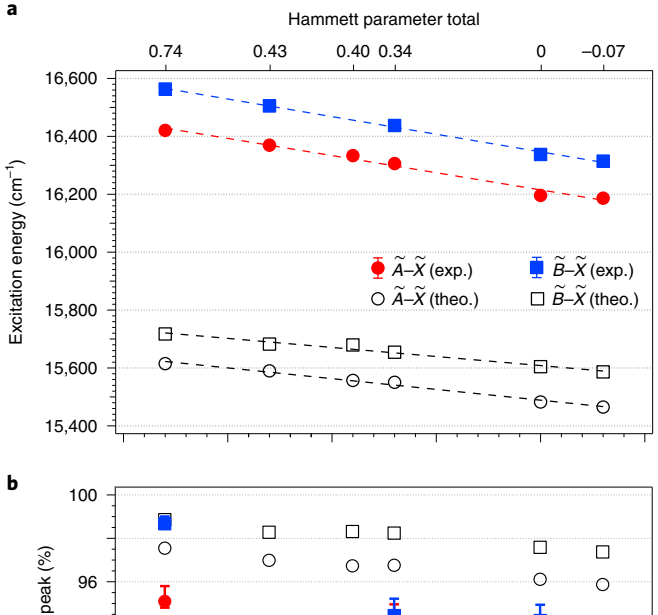
can be assigned to the ${}^B0^0_0$ decay. This excitation process is presumably due to collisions with hot reaction products before they are thermalized by the buffer gas. Finally, a weak peak at $-1,172\,\mathrm{cm}^{-1}$ is attributed to the stretching mode 24^0_1 , and the strong peak at $-584\,\mathrm{cm}^{-1}$ is assigned to CaF $A^2\Pi_{3/2}(\nu'=0) \to X^2\Sigma^+(\nu''=1)$ decay. A comparison of the experimental and theoretical frequencies of all observed modes is summarized in Supplementary Table 2.

Scaled VBRs and pK_a trends. As seen in the relative heights of the $^A0_0^0$ and $^B0_0^0$ peaks in Fig. 1d,e, both the $\widetilde{A}-\widetilde{X}$ and $\widetilde{B}-\widetilde{X}$ transitions are promising for optical cycling, as vibrational-state-preserving decays are strongly favoured. Because vibration-changing decays below the measurement sensitivity ($^{\sim}1\times 10^{-3}$) or obscured by other peaks may not have been observed, the ratio of the intensities of these peaks is not strictly a VBR (Supplementary Information). Therefore, to compare to theoretical calculations we plot the ratio of intensities of only the observed peaks in Fig. 2b,c. In general, Fig. 2b,c shows reasonable agreement between experiment and theory, other than the aforementioned underestimate of the decay to low-frequency bending modes (v_1 or v_2). The theoretical and observed values of the vibrational decay ratios of all observed modes are given in Supplementary Table 3.

To explore the effect of the ligand on the OCC, Fig. 3 plots the measured transition energies (also Supplementary Table 4) and estimated 0_0^0 VBRs as a function of the precursor p K_a in solution. The pK_a is a convenient parameter that indicates the strength of an acid R-OH, and therefore quantifies the electron-withdrawing capability of the R-O⁻ ligand. A smaller pK_a implies a more ionic Ca(I)-O bond in R-O-Ca. A similar metric to p K_a , shown on a second horizontal axis, is the Hammett parameter total²², which has been used in previous theoretical work¹⁵ and varies monotonically with the p K_a (Supplementary Table 5). As can be seen in Fig. 3a, the excitation energies follow a monotonic and apparently linear trend with pK_a . This behaviour is qualitatively understood as an increase in the HOMO-LUMO gap as the electron-withdrawing strength of the ligand increases²³, yielding more localized molecular orbitals on the Ca atom (Fig. 1b) with a trend towards the atomic Ca⁺ ion. The calculated $\widetilde{A} - \widetilde{B}$ energy differences are systematically smaller than the experimental values by ~5 meV, probably a result of the omission of spin-orbit coupling from the theoretical calculation²⁴.

Figure 3b shows the estimated 0_0^0 VBRs (Supplementary Table 3) as a function of pK_a . The 0_0^0 VBR for each transition is estimated by normalizing the observed 0_0^0 decay signal by the signal of all observed transitions plus an estimated contribution of the unobserved peaks (Methods and Supplementary Information). The error bars on each point represent the combination of the statistical standard error and the uncertainty from the unobserved peaks (Supplementary Tables 6 and 7). Systematic errors, discussed in the Methods and Supplementary Information, are expected to be smaller than a few percent.

Remarkably, across all six ligands and a considerable range of pK_a , the VBRs are relatively unchanged and always \gtrsim 90%, indicating that the OCC function can indeed be made orthogonal to the ligand molecule. The theoretical calculations in Fig. 3b show an increase in VBR for stronger acids, as previously predicted ¹⁵. This trend is consistent with the experimental data, and is understood as the localization of the electronic wavefunction on the Ca atom with a more ionic Ca(I)–O bond, leading to further isolation of the electronic and vibrational degrees of freedom ¹⁵. This suggests that, although an OCC can be successfully attached to a wide range of molecules, performance may still be optimized by choosing ligands with strong electron-withdrawing character. Deviation from this trend probably occurs in CaO-Ph-3-CF₃. Here, the lower symmetry and large electron inductive effect may lead to larger vibronic mixing between the \widetilde{A} and \widetilde{B} excited states, which can increase



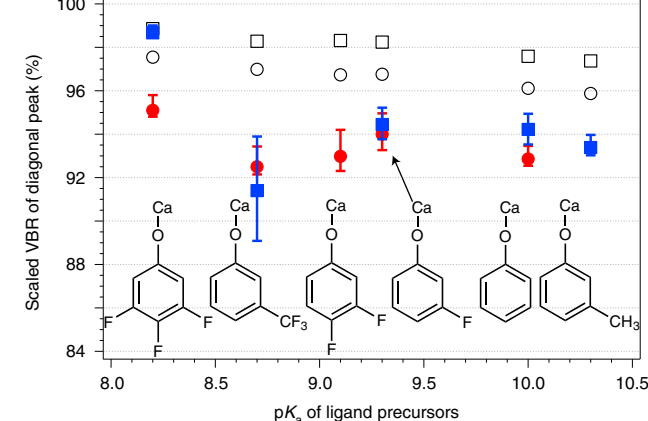


Fig. 3 | pK_a trends. \mathbf{a} , $\widetilde{A} = \widetilde{X}$ and $\widetilde{B} = \widetilde{X}$ transition energies versus pK_a for all molecular species studied here. The linear fits to the experimental data yield $E_{\widetilde{A}} = 17,400-118.0 \times pK_a$ (cm⁻¹) and $E_{\widetilde{B}} = 17,561-121.5 \times pK_a$ (cm⁻¹). \mathbf{b} , Scaled VBR for diagonal decay as a function of pK_a . The large error bar for the $\widetilde{B} \to \widetilde{X}$ decay of CaO-Ph-3-CF $_3$ is due to a partial spectral overlap with CaF. The pK_a and Hammett parameter can be linked by the derived Hammett equation (Supplementary Table 5).

vibration-changing decay. Our level of theory cannot capture this mixing and therefore would underestimate the effect.

Laser cooling and prospects. Together, these features illustrate that a quantum functional group, furnishing a means for gaining full quantum control of a wide range of molecules, should be possible. As an example, from the recorded structure and measured state lifetimes (Supplementary Fig. 1), we estimate that a magneto-optical trap of CaO-Ph-3,4,5-F₃ is possible using the $\widetilde{B}-\widetilde{X}$ transition with six to eight lasers (see Methods for further details)²⁵. Interestingly, this is similar to the number of lasers required in molecules with roughly an order of magnitude fewer vibrational modes²⁶. Furthermore, using the same laser system, single quantum states can be prepared via optical pumping and measured by state-resolved fluorescence with high fidelity.

The ability to laser-cool and prepare single quantum states of such 'large' molecules opens the door to a host of new science applications. The rich structures of these molecules allow robust encoding of quantum information²⁷ and provide new platforms for precision measurement and tests of fundamental physics^{28,29} as well as quantum simulation and computing^{30,31}. Ultracold organic hydrocarbons can be produced via zero-energy photofragmentation³² of those complexes and offer new opportunities for ultracold

NATURE CHEMISTRY ARTICLES

chemical reactions and collision studies³³. Furthermore, theoretical work suggests that the scheme demonstrated here can be continued to even larger molecules¹⁶ and extended to surfaces³⁴.

Conclusion

In summary, we have functionalized six precursor compounds (phenol, *m*-cresol, 3-fluorophenol, 3-(trifluoromethyl)phenol, 3,4,-difluorophenol and 3,4,5-trifluorophenol) with an optical cycling centre composed of a Ca(I)-O functional group. The resulting molecules were studied at cryogenic temperature via 2D and dispersed fluorescence spectroscopy. The excitation energies of the molecules showed a linear correlation with the pK_a of the organic precursors, providing a convenient way of discovering new molecules. Meanwhile, the vibrational branching ratios were largely unaffected by the choice of ligand and at a level sufficient for laser cooling and trapping as well as quantum state preparation and measurement. This demonstration of the orthogonality of the OCC function to the ligand function lays the groundwork for functionalizing molecules with quantum functional groups and establishes principles of chemical design that can be used to build molecules of increasing size, complexity and function for quantum science and technology.

Online content

Any methods, additional references, Nature Research reporting summaries, source data, extended data, supplementary information, acknowledgements, peer review information; details of author contributions and competing interests; and statements of data and code availability are available at https://doi.org/10.1038/s41557-022-00998-x.

Received: 24 January 2022; Accepted: 14 June 2022;

Published online: 25 July 2022

References

- Campisciano, V., Gruttadauria, M. & Giacalone, F. Modified nanocarbons for catalysis. ChemCatChem 11, 90–133 (2019).
- Wang, Q. & Astruc, D. State of the art and prospects in metal-organic framework (MOF)-based and MOF derived nanocatalysis. *Chem. Rev.* 120, 1438–1511 (2020).
- Liu, Y., Dong, X. & Chen, P. Biological and chemical sensors based on graphene materials. Chem. Soc. Rev. 41, 2283–2307 (2012).
- Saha, K., Agasti, S. S., Kim, C., Li, X. & Rotello, V. M. Gold nanoparticles in chemical and biological sensing. *Chem. Rev.* 112, 2739–2779 (2012).
- Guillemard, L., Kaplaneris, N., Ackermann, L. & Johansson, M. J. Late-stage C–H functionalization offers new opportunities in drug discovery. *Nat. Rev. Chem.* 5, 522–545 (2021).
- 6. Di Rosa, M. Laser-cooling molecules. Eur. Phys. J. D 31, 395-402 (2004).
- Shuman, E. S., Barry, J. F. & DeMille, D. Laser cooling of a diatomic molecule. *Nature* 467, 820–823 (2010).
- Anderegg, L. et al. Radio frequency magneto-optical trapping of CaF with high density. Phys. Rev. Lett. 119, 103201 (2017).
- Isaev, T. A. & Berger, R. Polyatomic candidates for cooling of molecules with lasers from simple theoretical concepts. *Phys. Rev. Lett.* 116, 063006 (2016).

 Vilas, N. B. et al. Magneto-optical trapping and subdoppler cooling of a polyatomic molecule. Nature 606, 70–74 (2022).

- Kozyryev, I., Baum, L., Matsuda, K. & Doyle, J. Proposal for laser cooling of complex polyatomic molecules. Chem. Phys. Chem. 17, 3641–3648 (2016).
- Mitra, D. et al. Direct laser cooling of a symmetric top molecule. Science 369, 1366–1369 (2020).
- Ivanov, M. V., Bangerter, F. H. & Krylov, A. I. Towards a rational design of laser-coolable molecules: insights from equation-of-motion coupled-cluster calculations. *Phys. Chem. Chem. Phys.* 21, 19447–19457 (2019).
- Ivanov, M. V., Bangerter, F. H., Wójcik, P. & Krylov, A. I. Toward ultracold organic chemistry: prospects of laser cooling large organic molecules. *J. Phys. Chem. Lett.* 11, 6670–6676 (2020).
- Dickerson, C. E. et al. Franck-Condon tuning of optical cycling centers by organic functionalization. Phys. Rev. Lett. 126, 123002 (2021).
- Dickerson, C. E. et al. Optical cycling functionalization of arenes. J. Phys. Chem. Lett. 12, 3989–3995 (2021).
- Hutzler, N. R., Lu, H.-I. & Doyle, J. M. The buffer gas beam: an intense, cold, and slow source for atoms and molecules. Chem. Rev. 112, 4803–4827 (2012).
- Domcke, W., Cederbaum, L., Köppel, H. & Von Niessen, W. A comparison of different approaches to the calculation of Franck-Condon factors for polyatomic molecules. *Mol. Phys.* 34, 1759–1770 (1977).
- 19. Fischer, G. Vibronic Coupling: The Interaction Between the Electronic and Nuclear Motions (Academic, 1984).
- 20. Paul, A. C. et al. Laser-induced fluorescence and dispersed-fluorescence spectroscopy of the $\widetilde{A}^2E-\widetilde{X}^2A_1$ transition of jet-cooled calcium methoxide (CaOCH₃) radicals. *J. Chem. Phys.* **151**, 134303 (2019).
- Dagdigian, P. J. State-resolved collision-induced electronic transitions. Annu. Rev. Phys. Chem. 48, 95–123 (1997).
- Hammett, L. P. The effect of structure upon the reactions of organic compounds. Benzene derivatives. J. Am. Chem. Soc. 59, 96–103 (1937).
- Mao, Y., Head-Gordon, M. & Shao, Y. Unraveling substituent effects on frontier orbitals of conjugated molecules using an absolutely localized molecular orbital based analysis. *Chem. Sci.* 9, 8598–8607 (2018).
- Liu, J. Rotational and fine structure of open-shell molecules in nearly degenerate electronic states. J. Chem. Phys. 148, 124112 (2018).
- Augenbraun, B. L., Doyle, J. M., Zelevinsky, T. & Kozyryev, I. Molecular asymmetry and optical cycling: laser cooling asymmetric top molecules. *Phys. Rev. X* 10, 031022 (2020).
- Baum, L. et al. Establishing a nearly closed cycling transition in a polyatomic molecule. *Phys. Rev. A* 103, 043111 (2021).
- Albert, V. V., Covey, J. P. & Preskill, J. Robust encoding of a qubit in a molecule. *Phys. Rev. X* 10, 031050 (2020).
- Augenbraun, B. L. et al. Laser-cooled polyatomic molecules for improved electron electric dipole moment searches. New J. Phys. 22, 022003 (2020).
- Hutzler, N. R. Polyatomic molecules as quantum sensors for fundamental physics. Quantum Sci. Technol. 5, 044011 (2020).
- Blackmore, J. A. et al. Ultracold molecules for quantum simulation: rotational coherences in CaF and RbCs. Quantum Sci. Technol. 4, 014010 (2018).
- Yu, P., Cheuk, L. W., Kozyryev, I. & Doyle, J. M. A scalable quantum computing platform using symmetric-top molecules. *New J. Phys.* 21, 093049 (2019).
- Lane, I. C. Ultracold fluorine production via doppler cooled BeF. Phys. Chem. Chem. Phys. 14, 15078–15087 (2012).
- Balakrishnan, N. Perspective: ultracold molecules and the dawn of cold controlled chemistry. J. Chem. Phys. 145, 150901 (2016).
- Guo, H. et al. Surface chemical trapping of optical cycling centers. Phys. Chem. Chem. Phys. 23, 211–218 (2021).

Publisher's note Springer Nature remains neutral with regard to jurisdictional claims in published maps and institutional affiliations.

© The Author(s), under exclusive licence to Springer Nature Limited 2022

Methods

Production of molecules. The studied molecules were produced by the reaction of Ca atoms with ligand precursors in a cryogenic buffer-gas cell operated at ~9 K (ref. ¹⁷). Five precursor molecules—phenol, *m*-cresol, 3-fluorophenol, 3-(trifluoromethyl)phenol and 3,4,5-trifluorophenol—were purchased commercially and used without further purification. Gas-phase Ca atoms were introduced into the buffer gas by laser ablation of a metallic Ca target using the second harmonic of a pulsed Nd:YAG laser (with approximate parameters of 20-mJ pulse energy, 100-µm spot size, 5-ns pulse length and 10-Hz repetition rate). The position of the ablation laser was continuously swept over the target with a moving mirror to avoid ablation-induced yield drifts. A reservoir containing the ligand precursors was heated to a temperature between 300 K and 350 K to maintain a vapour pressure of 3–5 torr (melting points of precursors are provided in Supplementary Table 5). The resulting vapour was flowed into the cryogenic cell via a thermally isolated, heated fill line. The calcium-bearing reaction products (CaO-Ph-X) were cooled via collisions with He buffer gas of density ~10¹⁵⁻¹⁶ cm⁻³.

Spectroscopy system details. The resulting CaO-Ph-X molecules were studied using 2D spectroscopy via excitation and dispersed fluorescence $^{36-38}$, DLIF spectroscopy and radiative decay. A tunable, pulsed OPO (with approximate parameters of 5-cm $^{-1}$ linewidth, 10-ns pulse duration and 1-mJ pulse energy) illuminated the molecules at a delay of ~1 ms after the ablation pulse. The OPO wavelength was continuously tunable from 500 nm to 700 nm and the absolute wavelength was determined by a spectrum analyser with a measurement accuracy of 0.5 nm. Molecular fluorescence was collected into a 0.67-m focal length Czerny-Turner style monochromator (numerical aperture ≈ 0.1) equipped with a 300 lines mm $^{-1}$ grating (500-nm blaze). The dispersed fluorescence was imaged onto a gated ICCD cooled to −30 °C. Given the system passband, an ~80-nm-wide spectral region of the DLIF could be recorded in a single image. The spectral resolution of the spectrometer was ~0.5 nm.

Theoretical calculations. We label the electronic symmetries according to representations of the $C_{2\nu}$ point group, although for molecules with C_s symmetry the appropriate symmetry species are A' and A''.

All molecular optimized geometries and frequency calculations were obtained on a superfine grid in Gaussian16 at the PBE0-D3/def2-tzvppd level of theory using density functional theory (DFT)/time-dependent DFT methods³⁹⁻⁴². Franck-Condon factors (FCFs) were calculated within the parallel harmonic approximation with ezFCF⁴³. Due to the isolated density of the OCCs and the rigidity of the molecule, the parallel harmonic approximation is expected to be reliable. However, anharmonicity effects and potential errors are discussed further in a previous paper¹⁵. Additionally, FCFs calculated with DFT missed vibronic coupling effects due to the single reference nature of the DFT formalism. Higher-level theory is needed to express vibronic coupling effects more accurately, but we find DFT to be a suitable qualitative approximation to predict FCFs for these molecules. The theoretical VBRs in Supplementary Tables 3 and 8–10 are converted by the calculated FCFs with the formula²⁵

$$b_{i\nu',f\nu''} = \frac{I_{\nu',f\nu''}}{\sum_{f'}I_{n',f\nu''}} = \frac{A_{\nu',f\nu''}}{\sum_{f'}I_{A',f\nu''}}$$

$$= \frac{|\mu_{\nu',f,\nu'}|^2 \times (\nu_{\nu',f\nu'})^3}{\sum_{f'}I_{\mu',f\nu'}|^2 \times (\nu_{\nu',f\nu'})^3}$$

$$\approx \frac{\text{FCF}_{\nu',f\nu'} \times \nu_{\lambda',f\nu''}^3}{\sum_{f'}\text{FCF}_{\nu',f\nu'} \times \nu_{\lambda',f\nu''}^3}$$
(1)

where i and f indicate the initial and final states, respectively, $b_{i\nu',f\nu''}$ is the branching ratio, $I_{i\nu',f\nu''}$ is the intensity, $A_{i\nu',f\nu''}$ is the Einstein coefficient for spontaneous emission, $\mu_{i\nu',f\nu''}$ is the transition dipole moment and $\nu_{i\nu',f\nu''}$ is the transition frequency.

Systematic error. In addition to the statistical uncertainty, there are several sources of systematic uncertainty (Supplementary Table 6). First, vibration-changing decays with a strength below our experimental sensitivity (Supplementary Tables 8–10) can lead to a VBR error of up to 3%. Second, calibration error in the wavelength response of our instrument, including the imaging system, spectrometer and ICCD camera, could lead to a VBR error of up to ~1%. Third, diagonal excitations from excited vibrational levels and subsequent decays can skew the measured VBRs if the excited states' VBRs differ from those of the ground state. Because the molecules are thermalized with helium buffer gas, the population of excited vibrational levels is small and this error is estimated to be smaller than 0.5%. Finally, the measured laser power fluctuations could lead to an error of up to 0.5% and the fitting model could lead to VBR errors by at most 1%. Further details are provided in the Supplementary Information.

Laser-cooling estimates. With the measured diagonal VBRs of all six molecules being ≥90% (Fig. 3 and Supplementary Table 3), a quantum functional group that furnishes a means for gaining full quantum control of a wide range of molecules should be possible. An estimate of the feasibility of such a scheme can be obtained

by considering the number of lasers required to scatter on order of 1,000 photons from a molecule via the OCC; this number of scattered photons is typically enough to realize laser cooling and/or high-fidelity detection 12,28,44 . For example, for the $\widetilde{B}-\widetilde{X}$ transition in CaO-Ph-3,4,5-F₃, three lasers to 'repump' the observed decays to ν_{e_3} , ν_{24} and ν_{16} should be sufficient. Additional lasers may be necessary to repump decays that change the rotational state of the molecule. And although the details depend on pending high-resolution spectroscopy, we estimate that, in total, approximately six to eight lasers would be necessary to scatter ~1,000 photons. Interestingly, this is similar to the number of lasers required to achieve an equivalent photon budget in molecules with roughly an order of magnitude fewer vibrational modes 26,45 . Finally, given that we have measured the lifetime of these excited states to be roughly 20–30 ns (Supplementary Fig. 1), a strong scattering force can be expected, and techniques like laser cooling should be applicable.

2D and DLIF spectra of other molecules. The 2D and DLIF spectra of the other five molecules—CaO-Ph, CaO-Ph-3-CH₃, CaO-Ph-3-F, CaO-Ph-3-CF₃ and CaO-Ph-3,4-F₂—are presented in Extended Data Fig. 1. The 2D spectra were recorded by monitoring the emission wavelength when scanning the excitation wavelength at a step size of 0.2 nm in the region of 600–620 nm. Besides the transition bands from the molecular species of interests, indicated by green dotted lines, those from unwanted species of Ca, CaOH and CaF, indicated by orange dashed lines, are also observed. The Ca atom is directly produced by laser ablation, and CaOH and CaF are formed by the reactions with water or precursor ligands. By putting the laser wavelengths at the excitation bands of CaO-Ph-X (green dotted lines), the respective DLIF spectra are obtained for both $\widetilde{A} \to \widetilde{X}$ and $\widetilde{B} \to \widetilde{X}$ transitions. All spectra are fitted with Pearson functions (red traces) to extract VBRs. In comparison to the theoretical vibrational frequencies (Supplementary Table 1) and VBRs (Supplementary Tables 8–10), the resolved vibrational peaks can be assigned to different vibrational modes, as labelled in the spectra.

Extended Data Fig. 1a shows the 2D spectrum of CaO-Ph. Besides the two bands from CaO-Ph indicated by the green dotted lines, several bands are observed for Ca and CaOH. The strong CaOH band at around 617 nm is overlapped with the CaO-Ph $\widetilde{A} = \widetilde{X}$ band, which results in many CaOH peaks, as denoted by asterisks in the dispersed spectrum of CaO-Ph in Extended Data Fig. 1b. The origin peak, labelled as ${}^{A}0_{0}^{0}$, represents the fluorescence decay from the excited $\widetilde{A}(\nu'=0)$ state to the ground \widetilde{X} (v''=0) state. The shifts and relative intensities of peaks at -312 cm⁻¹ and -627 cm⁻¹ agree well with simulations and they can be assigned to the Ca–O stretching modes ν_4 (314 cm⁻¹) and ν_9 (631 cm⁻¹), respectively. The weak peak at $-878 \,\mathrm{cm}^{-1}$ is assigned to ν_{13} (903 cm⁻¹), and a shelf peak at $-44 \,\mathrm{cm}^{-1}$ is from the bending mode ν_2 (61 cm⁻¹). The peak at the positive shift of $117 \,\mathrm{cm}^{-1}$ is ascribed to the $\widetilde{B}(v'=0) \to \widetilde{X}(v''=0)$ decay. The presence of the excited \widetilde{B} state when exciting to the \widetilde{A} state has been observed for all molecules, and is probably due to the buffer-gas collision-induced excitation. Without the contamination of CaOH, the $\widetilde{B} \to \widetilde{X}$ spectrum of CaO-Ph in Extended Data Fig. 1c is straightforward to assign. The same vibrational modes are resolved and the respective peaks are labelled as ${}^{B}2_{1}^{0}$, ${}^{B}4_{1}^{0}$, ${}^{B}9_{1}^{0}$ and ${}^{B}13_{1}^{0}$. Besides, the shift of the peaks labelled as ${}^{A}0_{0}^{0}$ at $-138\,\mathrm{cm}^{-1}$, not matching the frequencies of any vibrational modes, is due to the collision-induced relaxation of $B(v'=0) \to A(v'=0)$, followed by fluorescence decay to $\widetilde{X}(v''=0)$.

The DLIF spectra of CaO-Ph-3- $\dot{C}H_3$ are displayed in Extended Data Fig. 1e,f. The excitation wavelength of $\widetilde{A}\leftarrow\widetilde{X}$ at 617.80 nm can also excite the CaOH transition $\widetilde{A}^2\Pi_{1/2}(02^20)\leftarrow\widetilde{X}^2\Sigma^+$ (100), which results in a broad peak, labelled by an asterisk, at around $-100\,\mathrm{cm}^{-1}$ and contributes to the diagonal peak. The difficulty to subtract the CaOH contribution makes it impossible to estimate the VBR for the $\widetilde{A}\to\widetilde{X}$ of CaO-Ph-3-CH₃. The two peaks at $-285\,\mathrm{cm}^{-1}$ and $-327\,\mathrm{cm}^{-1}$ are assigned to stretching modes ν_6 and ν_7 , respectively, by comparison to the theoretical frequencies (Supplementary Table 1) and relative VBRs (Supplementary Table 8). The $\widetilde{B}\to\widetilde{X}$ is more complicated due to the relaxation to A and the overlapped Ca transition lines. Four vibrational peaks have been observed and labelled as $^B6_1^0$, $^B7_1^0$, $^B12_1^0$ and $^B14_1^0$, which are predicted to be the top four off-diagonal modes. The relaxations to \widetilde{A} are confirmed with the observed peaks of $^A0_0^0$, $^A6_1^0$ and $^A7_1^0$. The plus symbols label the peaks due to decays from Ca 3S_1 , generated by laser ablation, to Ca 3P_1 (J=0, 1, 2). The VBR calculations have subtracted the contribution from Ca emissions.

Extended Data Fig. 1g illustrates the 2D spectrum of CaO-Ph-3-F. Besides the strong bands from CaF and CaO-Ph-3-F, there are two weak bands from CaO-Ph, which is the by-product of the reaction between Ca and 3-fluorophenol. The dispersed spectrum obtained by pumping the $\widetilde{A}\leftarrow\widetilde{X}$ transition resolves five off-diagonal vibrational modes, including one bending mode ν_1 and four stretching modes ν_5,ν_6,ν_{10} and ν_{14} . The higher intensity of peak $^A6^0_1$ than peak $^A5^0_1$, which is contrary to the theoretical VBRs, is due to the contribution of CaOH $\widetilde{A}^2\Pi_{1/2}(010)\to\widetilde{X}^2\Sigma^+(000)$ also has a weak contribution to the diagonal peak. In Extended Data Fig. 1i, the four same vibrational peaks, labelled as $^B1^0_1$, $^B5^0_1$, $^B6^0_1$ and $^B10^0_1$, are observed for the $\widetilde{B}\to\widetilde{X}$ transition and agree perfectly with the theoretical predictions (blue lines). The additional relaxation peak $^A0^0_0$ is also observed without surprise.

The spectra of CaO-Ph-3-CF₃ are more complicated due to the non-planar structure introduced by the substituent CF₃ group. By comparing to the theoretical

NATURE CHEMISTRY ARTICLES

frequencies (Supplementary Table 1) and VBRs (Supplementary Table 9), seven vibrational peaks have been assigned and labelled in the dispersed spectrum of $\widetilde{A} \to \widetilde{X}$ in Extended Data Fig. 1k. For the $\widetilde{B} \to \widetilde{X}$ decay in Extended Data Fig. 1l, five vibrational peaks are assigned as $^B2_1^0, ^B7_1^0, ^B9_1^0, ^B15_1^0$ and $^B23_1^0$, and five additional peaks are observed for the $\widetilde{A} \to \widetilde{X}$ transition due to relaxation from \widetilde{B} . The CaF peak from the transition of $A^2\Pi_{1/2}(\nu'=0) \to X^2\Sigma^+(\nu''=1)$ is also observed, in coincidence. The CaF intensity in the diagonal peak is subtracted when calculating the VBR.

The reaction of 3,4,5-trifluorophenol with Ca can produce two by-products, CaO-Ph-3,4-F₂ and CaO-Ph-3,5-F₂, with one F atom reacted. The 2D spectrum in Extended Data Fig. 1m shows a new band at 612.0 nm besides those from CaO-Ph-3,4,5-F₃ and CaF. Because 3,5-difluorophenol has a lower pK_a value than 3-(trifluoromethyl)phenol (Supplementary Table 5), the corresponding product CaO-Ph-3,5-F₂ is supposed to have a higher transition energy than CaO-Ph-3-CF₃ based on the trend of transition energies versus pK_a in Fig. 3a. The lower transition energy of this band at 612.0 nm than the $\widetilde{A} - \widetilde{X}$ transition of CaO-Ph-3-CF₃ at 610.90 nm excludes the possibility of CaO-Ph-3,5-F₂. Therefore, this new band is assigned to the $\widetilde{A} = \widetilde{X}$ transition of CaO-Ph-3,4-F₂, which follows the trend of transition energies versus pK_a in Fig. 3a. Besides, the observed vibrational peaks with shifts of -275 cm⁻¹ and -292 cm⁻¹ in Extended Data Fig. 1n agree well with the theoretical frequencies of Ca–O stretching modes ν_5 (278 cm⁻¹) and ν_6 (293 cm⁻¹) of CaO-Ph-3,4-F₂, respectively, as listed in Supplementary Table 1. The relative intensities of these two peaks are also in good agreement with the theoretical VBRs (blue lines, Supplementary Table 10). A small shoulder near the diagonal main peak is from the in-plane bending mode ν_2 .

The transition energies of all molecules are summarized in Supplementary Table 4. The VBRs of all peaks are summarized in Supplementary Table 3 and the resolved vibrational frequencies are summarized in Supplementary Table 2. Supplementary Fig. 2 presents the corresponding vibrational displacements.

Data availability

The experimental datasets and codes for Figs. 1–3 and Extended Data Fig. 1 are available as source data and from the online Zenodo repository at https://zenodo.org/record/6578610#.YsRnod8o9PY. Other data supporting the findings of this study are available in the Supplementary Information. Source data are provided with this paper.

References

- Reilly, N. J., Schmidt, T. W. & Kable, S. H. Two-dimensional fluorescence (excitation/emission) spectroscopy as a probe of complex chemical environments. J. Phys. Chem. A 110, 12355–12359 (2006).
- Gascooke, J. R., Alexander, U. N. & Lawrance, W. D. Two-dimensional laser induced fluorescence spectroscopy: a powerful technique for elucidating rovibronic structure in electronic transitions of polyatomic molecules. *J. Chem. Phys.* 134, 184301 (2011).
- Kokkin, D. L., Steimle, T. C. & DeMille, D. Branching ratios and radiative lifetimes of the *U, L* and *I* states of thorium oxide. *Phys. Rev. A* 90, 062503 (2014).
- 38. Augenbraun, B. L. et al. Observation and laser spectroscopy of ytterbium monomethoxide, YbOCH₃. *Phys. Rev. A* **103**, 022814 (2021).

- Perdew, J. P., Ernzerhof, M. & Burke, K. Rationale for mixing exact exchange with density functional approximations. *J. Chem. Phys.* 105, 9982–9985 (1996).
- Grimme, S., Antony, J., Ehrlich, S. & Krieg, H. A consistent and accurate ab initio parametrization of density functional dispersion correction (DFT-D) for the 94 elements H-Pu. J. Chem. Phys. 132, 154104 (2010).
- Rappoport, D. & Furche, F. Property-optimized Gaussian basis sets for molecular response calculations. J. Chem. Phys. 133, 134105 (2010).
- 42. Frisch, M. J. et al. Gaussian 16, revision C.01 (Gaussian, 2016).
- Gozem, S. & Krylov, A. I. The ezSpectra Suite: an easy-to-use toolkit for spectroscopy modeling. Wiley Interdiscip. Rev. Comput. Mol. Sci 12, e1546 (2021).
- Cheuk, L. W. et al. Λ-enhanced imaging of molecules in an optical trap. Phys. Rev. Lett. 121, 083201 (2018).
- Zhang, C. et al. Accurate prediction and measurement of vibronic branching ratios for laser cooling linear polyatomic molecules. J. Chem. Phys. 155, 091101 (2021).

Acknowledgements

We thank T. C. Steimle for sharing critical equipment and for useful discussions and also N. Vilas and Y. Bao for helpful discussions. This work was supported in part by the National Science Foundation (grants nos. PHY-1255526, PHY-1415560, PHY-1912555, PHY-2110421, CHE-1900555, DGE-1650604, DGE-2034835 and OMA-2016245), the Army Research Office (grants nos. W911NF-15-1-0121, W911NF-14-1-0378, W911NF-13-1-0213, W911NF-17-1-0071 and W911NF-19-1-0297), AFOSR (grant no. FA9550- 20-1-0323) and the US Department of Energy, Office of Science, Basic Energy Sciences (award no. DE-SC0019245).

Author contributions

A.N.A., W.C.C., J.R.C., J.M.D. and E.R.H. conceived the idea. D.M., B.L.A. and Z.D.L. constructed the vacuum, cryogenic and spectroscopic apparatus under the supervision of J.M.D. G.-Z.Z. and G.L. explored the initial production method. G.-Z.Z., D.M. and Z.D.L. acquired all the experimental data. C.E.D. performed all calculations. Z.D.L., D.M. and M.J.F. built the Pearson function to fit peaks in all DLIF spectra. G.-Z.Z. and D.M. analysed all data, with useful contributions from B.L.A., Z.D.L., W.C.C. and E.R.H. G.-Z.Z., D.M. and E.R.H. prepared the manuscript with contributions from all authors. The research was coordinated by W.C.C., J.M.D. and E.R.H.

Competing interests

The authors declare no competing interests.

Additional information

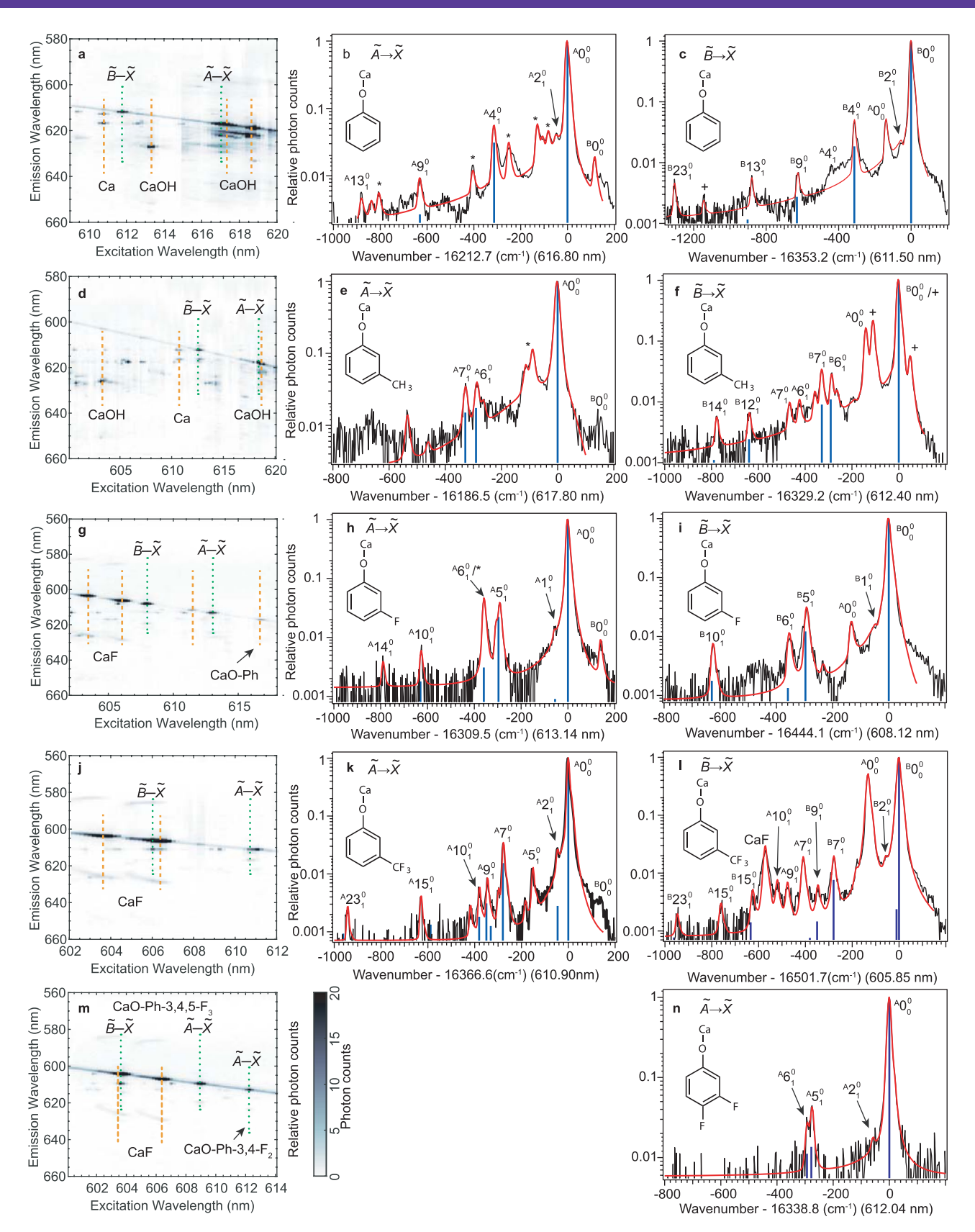
Extended data is available for this paper at https://doi.org/10.1038/s41557-022-00998-x.

Supplementary information The online version contains supplementary material available at https://doi.org/10.1038/s41557-022-00998-x.

Correspondence and requests for materials should be addressed to Eric R. Hudson.

Peer review information *Nature Chemistry* thanks Jinjun Liu and the other, anonymous, reviewer(s) for their contribution to the peer review of this work.

Reprints and permissions information is available at www.nature.com/reprints.



Extended Data Fig. 1 | 2D and DLIF spectra of all other five molecules. a-c, CaO-Ph. d-f. CaO-Ph-3-CH₃. g-i, CaO-Ph-3-F. j-l, CaO-Ph-3-CF₃. m-n, CaO-Ph-3,4-F₂. In the 2D spectra, the orange dashed lines mark features due to CaOH or CaF, while the green dotted lines indicate features from CaO-Ph-X species. In the corresponding dispersed LIF spectra, the experimental curves (black) are fitted with Pearson functions (red). The blue sticks illustrate the vibrational branching ratios of different vibrational modes. The assignments of resolved vibrational peaks are also given. The symbols * and + indicate features due to CaOH and Ca, respectively.